GRUPO ESPAÑOL CARBÓN
www.gecarbon.org

BOLETIN del Grupo Español del Carbón

ISSN 2172 - 6094
nº 38/Diciembre 2015

INDICE

Editorial

En este número tienen de nuevo especial relevancia los trabajos recibidos desde Hispanoamérica. Quiero, por tanto, agradecer las colaboraciones recibidas desde Colombia, específicamente, a través del Prof. Farid Cortés (Editor Invitado), de la Universidad Nacional de Colombia (Sede Medellín), que nos muestra algunas de las líneas de investigación que están desarrollando.

Anteriormente el número 36, coordinado por el Profesor Roberto Leyva, contenía específicamente trabajos desarrollados por distintos Grupos de Investigación mexicanos.

Aprovecho esta oportunidad para felicitar a dichos grupos por la reciente fundación de la **Asociación Mexicana de Carbono** (**AMEXCarb)**, seguro que tendrá mucho éxito científico.

Agradecer también a su Presidente, el Profesor René Rangel, no solo la amabilidad de enviarnos una reseña informándonos del acto, sino también sus colaboraciones anteriores.

La AMEXCarb trabajará dentro la Federación Latinoamericana de Carbono (FLC), constituida por las Asociaciones de Argentina, Brasil, Chile, Colombia, México y Uruguay. A todos ellos se les brinda también este Boletín como medio para el establecimiento de colaboraciones y difusión de resultados.

Agradecer también las reseñas de Tesis Doctorales recibidas, el empuje de los jóvenes investigadores, y su capacidad de mostrarnos su trabajo en los distintos Centros de Investigación. Me gustaría pedir, una vez más, la colaboración de todos los socios del GEC respecto al envío de comunicaciones, noticias, reseñas de Tesis, Congresos a los que asistáis, premios recibidos, etc.

En esta línea, de nuevo, para cerrar, más felicitaciones. Felicitar pues a Ana Arenillas y Angel Menendez por su premio, fruto de su buen hacer, y a Miguel Montes, por contárnoslo. Os animo a que hagáis lo mismo.

F.J. Maldonado Hódar

Effect of the Temperature in Water Adsorption onto Sub-Bituminous Coal

Esteban A. Taborda[1], Camilo A. Franco Ariza[1], William A. Jurado[2], Nashaat N. Nassar[3] and Farid B. Cortés[1,*]

[1] Grupo de Investigación en Yacimientos de Hidrocarburos, Facultad de Minas, Universidad Nacional de Colombia Sede Medellín, Kra 80 No. 65-223, Medellín, Colombia. Email: fbcortes@unal.edu.co.

[2] Departamento de Optimización de Procesos, Grupo ARGOS S.A, Colombia.

[3] Department of Chemical and Petroleum Engineering, University of Calgary, 2500 University Drive NW, Calgary, Alberta, Canada. Email: nassar@ucalgary.ca, Fax: +14032103973, Phone: +14032109772

Abstract

The presence of water in coal presents a technological challenge for its industrial use in energetic processes. Therefore, this study aims to study the temperature effect on the water adsorption onto coals. A Colombian bituminous coal was used as sample. The coal was characterized by nitrogen adsorption at 77 K (S_{BET}), Scanning electron microscopy (SEM), Fourier transform infrared (FT-IR) spectroscopy, elemental analysis (C-H-N elemental). The results showed that the water uptake increased as the vapor pressure increased. The Talu and Meunier model [1] was used to fit the adsorption isotherms, and the mean square root error (MSRE%) was lower than 10%. Additionally, the Gibbs free energy was found to have negative values, which corroborates the spontaneous adsorption process.

KEYWORDS

Adsorption, Coal, Isotherm, Water Uptake

1. Introduction

Coal is the most abundant fossil fuel on earth and is one of the main energy resources [2]. Global coal production is expected to increase by 30% and reach a maximum between 2020 and 2050 [2, 3]. Colombia has been shown to have the largest coal reserves in South America and is ranked eleventh globally [2] [2-4]. Nearly 85% of global coal reserves correspond to sub-bituminous and brown coals [2, 3]. Both of these coal types have active sites resulting in high water content due to their high affinity for polar molecules [5, 6]. The presence of water in coals presents several challenges for its application, as follows: 1) The risk for spontaneous combustion increases due to the oxidation of carbonaceous material in the coal at room temperature. This occurs when the coal is exposed to air and undergoes exothermic chemisorption of oxygen. Large coal stockpiles, especially those stored for long periods, may develop hot spots because of self-heating [7-9] caused by the adsorption/desorption of water on coal [10]; 2) The industrial costs for coal transportation have increased; and 3) A high amount of energy is required for coal drying via the thermal processes. The amount of water present in the coal is obtained naturally and from the chemical conversion of hydrogen (in the fuel) to water, which reflects the net heating value (NHV) of the coal [11]. The goal of this study is evaluate the temperature effect on the adsorption of water onto Colombian sub-bituminous coal. Different water adsorption isotherms were obtained at 21°C, 40°C and 50°C. The isotherms were phenomenologically described by the Talu and Meunier model for understanding the behavior of auto-associative molecules like water on coal [1]. Coal sample considered in this study were characterized using FTIR analysis, elemental analysis (C-H-N), Brunauer–Emmett–Teller (BET) surface area analysis by nitrogen physisorption at 77 K and NHV. Additionally, the values of the thermodynamic properties of water adsorption on coal were calculated.

2. Experiments

2.1 Coal preparation

A coal sample was obtained from the Cordoba region in northwestern Colombia and was used in this study. The coal sample preparation was performed by separating and quartering the sample four times. The particle size was subsequently reduced to approximately 250 mm using a jaw crusher and a ball mill, according to ASTM D2013-01 method. The coal was then dried in air at 120°C for 12 h and was transferred on a dewatering system to reach room temperature.

2.2 Coal characterization

The coal samples were characterized before and after impregnation. Elemental analysis was performed using a 5000A TOC (CHN Shimadzu, Japan) for obtaining C-H-N elements; the oxygen element was obtained by difference. N2 physisorption at 77 K was performed using an ASAP 2010 (Micromeritics, USA). The surface area (SBET) was obtained after degassing the sample for approximately 12 h at 140°C under high vacuum (10-6 mbar). The SBET was estimated using the Brunauer, Emmett and Teller (BET) method [12-14]. The minimum limit for this instrument to reliably detect surface area is 1 m^2/g. To determine the functional groups present in the coal, each sample was characterized by infrared spectroscopy (IRAffinity-1S Shimadzu, Japan) [15-17]. Scanning electron microscope (JSM-5910JL, JEOL Japan) was used to obtain images of selected samples to confirm their non-porous structure.

2.3 Adsorption isotherms

The static thermogravimetric method was used for the construction of the adsorption isotherm at 21, 30, 40 and 50°C. This method involves determining the weight gain of the coal subjected to different water activities (Aw) at a defined temperature. Containers with eight supersaturated saline solutions that provided a range of water activity between 0.113 and 0.90 (Table 1) were placed in an oven at each temperature for 24 h. After saline solutions preparation, the activity was continuously measured until a constant value was reached. Then, 0.5 g sample of the coal was placed inside the eight containers until equilibrium is reached. The coal sample was weighed every 8 h with an analytical balance (OHAUS – accuracy of 0.0001

Table 1. Hygroscopic salt solutions to control water activity (Aw)

Salt	K_{ps} (g/100 ml H_2O)	Aw = P/P^{sat}
Lithium Chloride (LiCl)	83.2	0.113
Calcium Chloride ($CaCl_2$)	74.5	0.295
Magnesium Chloride ($MgCl_2$)	54.6	0.328
Potassium Carbonate (K_2CO_3)	112	0.432
Sodium Bromide (NaBr)	90.5	0.577
Sodium Nitrite ($NaNO_2$)	80.8	0.654
Sodium Chloride (NaCl)	39.8	0.753
Potassium Chloride (KCl)	34.2	0.843

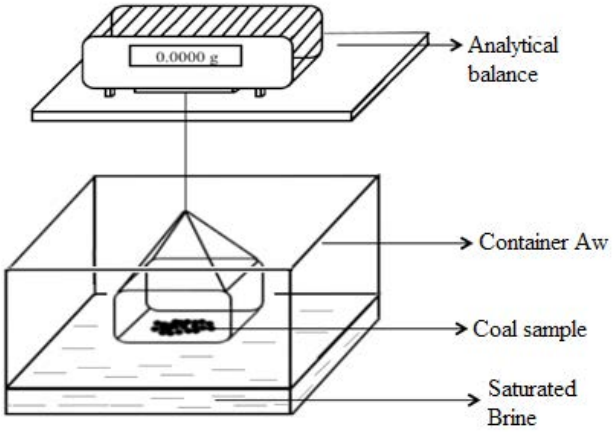

Figure 1. Schematic representation of the experimental set-up for adsorption isotherms construction.

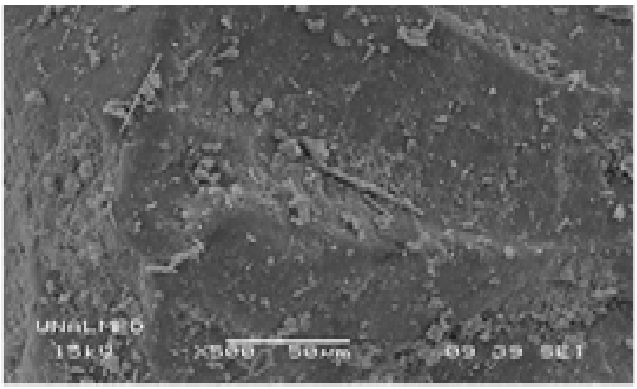

Figure 2. SEM images for selected coal sample.

Table 2. Elemental analysis (i.e., C-H-O-N) and estimated surface area.

Material	%Carbon (wt% C)	%Hydrogen (wt% H)	%Nitrogen (wt% N)	%Oxygen (wt% O)	O/C	H/C	S_{BET} (m^2/g)
Coal	64.79	5.15	1.96	28.11	0.43	0.079	4.94

g) until the sample weight did not vary by more than 1%. This procedure was performed by triplicated to confirm reproducibility, and standard deviations were calculated and presented as error bars on the isotherm figures. Finally, the amount of adsorbed water was estimated by calculating the difference between the initial and final sample weight. Water uptake (N_{ads}) was calculated as mg of water per g of dry coal [14, 18-25]. Figure 1 shows a schematic representation of the experimental setup. Table 1 shows the hygroscopic salts used to condition each system to the desired water activity.

3. Results and discussions

3.1 Samples characterization

Figure 2 shows scanning electron microscopy (SEM) images of coal. Accordingly, it seems that coal have a non-porous structure. Table 2 shows that the surface area (S_{BET}) of the coal. In addition, the low value of S_{BET} again supports that the materials are non-porous.

Table 2 also shows the elemental analysis of the coal samples.

3.2 Adsorption isotherms

Figure 3 shows the adsorption isotherm of water on coal at 21°C for a water activity between 0.10-0.90. The adsorption isotherms exhibited Type III behavior according to the IUPAC classification [1, 5]. The adsorption increased with increasing water activity. These findings are in good agreement with the available coal/water adsorption studies [23, 26-32]. The amount of water vapor in the sorption container increased due to increased vapor pressure (water activity). Collisions with the sample surface were highly favored, leading to a higher adsorbed amount. The resulting shape of the water sorption isotherm indicates a low affinity between the adsorbate and adsorbent, which mainly occurred at a low relative humidity (water activity). The behavior of the isotherm shows different interactions, including the water interaction with the active sites, along with multilayer adsorbed moisture on the surface of coal (Figure 3).

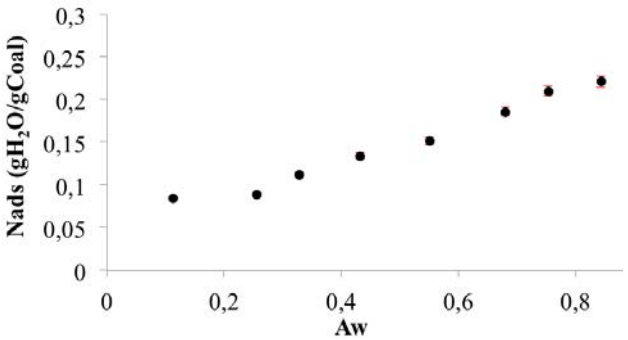

Figure 3. Water adsorption isotherm onto coal at 21°C.

The IR spectroscopy analysis shown in Figure 6 for sample after adsorption at Aw = 0.84. As seen, the signal near the 3300 cm^{-1} region indicates the presence of water [33]. It can be also seen that a signal intensity at approximately 3300 cm^{-1}. This is also representative of weather conditions in which water changes its intensity according to the sorption isotherm.

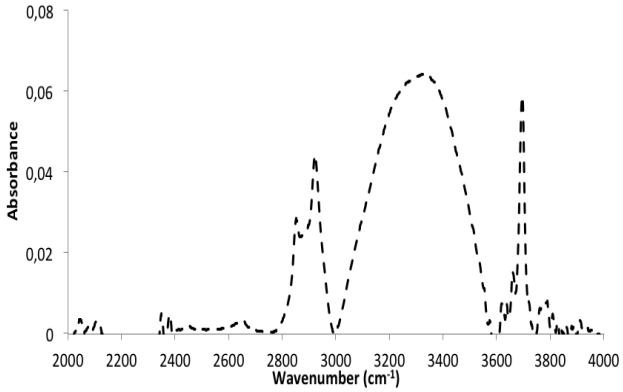

Figure 4. IR spectra for coal after adsorption at Aw = 0.84.

Adsorption isotherm were modeled using the Talu and Meunier model [1]. Talu and Meunier model [1] can be expressed as a general theory for the adsorption of self-associating molecules over solid structures. The approach is similar to the "*chemical*" interpretation of *non*-ideal vapor and liquid phases. The theory can explain the behavior of the Types I to V isotherms, including Type III isotherms characteristic of non-porous adsorbents, as it is the case of this work. Isothermal data are dependent on only three parameters: the inverse of Henry's law constant, the saturation capacity and the reaction constant for "cluster" [1]. The model is described as follows:

$$P = \frac{H\psi}{(1+K\psi)} Exp(\frac{\psi}{Nm}) \quad (1)$$

$$\psi = \frac{-1+\sqrt{(1+4K\varepsilon}}{2K} \quad (2)$$

$$\varepsilon = \frac{N_m N}{(N_m - \mathrm{N})} \quad (3)$$

where, *N (g/g)* is the adsorbed amount, N_m *(g/g)* is the saturation amount adsorbed by the monomer, *K (g/g)* is the reaction constant, *P (kPa)* is the equilibrium pressure, and *H (kPa)* is the Henry's law constant.

Figure 5 shows the comparison between experimental data and Talu and Meunier model fitting. Table 3 lists the values of the obtained parameters of the Talu and Meunier model. The parameter values are in agreement with the characteristics of the coals in which the *K* value is high. This indicates a rapid association of water molecules once the primary sites are occupied and is similar to the behavior described by the adsorption isotherms. On the other hand, the *H* values are also high (inverse of the common Henry's law constant), indicating that the steep rise in the water isotherm is delayed. Higher values of the *H* parameter indicate lower affinity of the water molecules for being in the adsorbed phase. The active sites are in locations that are not easily accessible to water. Low *K* values indicate that the primary sites are in widely varying space environments, resulting in a broadened step in the isotherm, which starts at lower pressures [1]. The differences between the N_m values for different coals simply correspond to the available adsorption space. This trend is also observed in the behavior of the isotherms (Figure 7).

3.2.1 Effect of the temperature

Figure 5 shows the amount adsorbed of water onto coal at 21, 30, 40 and 50°C for the sample together with the Talu and Meunier model fitting. Figure 8 shows that water adsorption is dependent on the system temperature. A Type III behavior according to the IUPAC classification [34] was exhibited, suggesting a multilayer adsorption for all evaluated temperatures. At a low water activity of less than 0.3, the behavior is described by the adsorption of water on the energy sites because of the preference and affinity of molecules for these sites [5, 6]. At high activity, the water molecules tend to form clusters around the high-energy sites via associations with hydrogen [1]. As expected, the equilibrium water content increased with increasing water activity. Furthermore, the amount of water adsorbed decreases with temperature because the higher energy weakens the interaction forces between the adsorbate and the adsorbent, thus facilitating water desorption [14]. With the data obtained through the sorption equilibrium tests at different temperatures, it is possible to calculate the thermodynamic properties of sorption.

The parameters for the Talu and Meunier model [1] at different temperatures for coal show a behavior of *H* that is only temperature dependent, as shown Table 3. Higher values suggest that there is a lower affinity between adsorbate and adsorbent at Henry's region [1]. When the temperature increases, the interactions between the coal and water are weakened, thus the interaction forces are reduced by the temperature. The parameter N_m is related to the maximum amount adsorbed, an increase in temperature favors the desorption, for this reason this parameter value decreases as the temperature increases. The *K* parameter is related to the degree of aggregation of water molecules on the surface of the adsorbent, hence the lower the amount adsorbed the less aggregation on the active sites, for that reason the parameter *K* decreases as the temperature increases.

3.3 Thermodynamic properties

To further understand the effect of temperature on adsorption, the thermodynamic properties of sorption were calculated. The isosteric heat of adsorption is the amount of energy dissipated during the adsorption process [6, 35]. It can also be defined as the amount of energy required for desorption. This can be calculated trough the commonly used Clausius-Clapeyron equation [18, 19, 21, 22, 35-37]. The isosteric heat (Q_{isos}) of adsorption in units of Cal/g can be estimated based on the established equilibrium between the condensed phase and gas phase [14]. This is shown in eq. 3:

$$Q_{isos} = \left(\frac{v_n}{v_g} - 1\right) RZ \left(\frac{\partial \ln P}{\partial\left(\frac{1}{T}\right)}\right)_{Nads} \quad (4)$$

where *P (kPa)* and *T (K)* are equilibrium pressure and temperature, respectively. *R* is the universal gas constant, *Z* is the compressibility factor V_n *(m³/g)* and V_g *(m³/g)* are the partial volume of the adsorbed species and of the gas phase respectively.

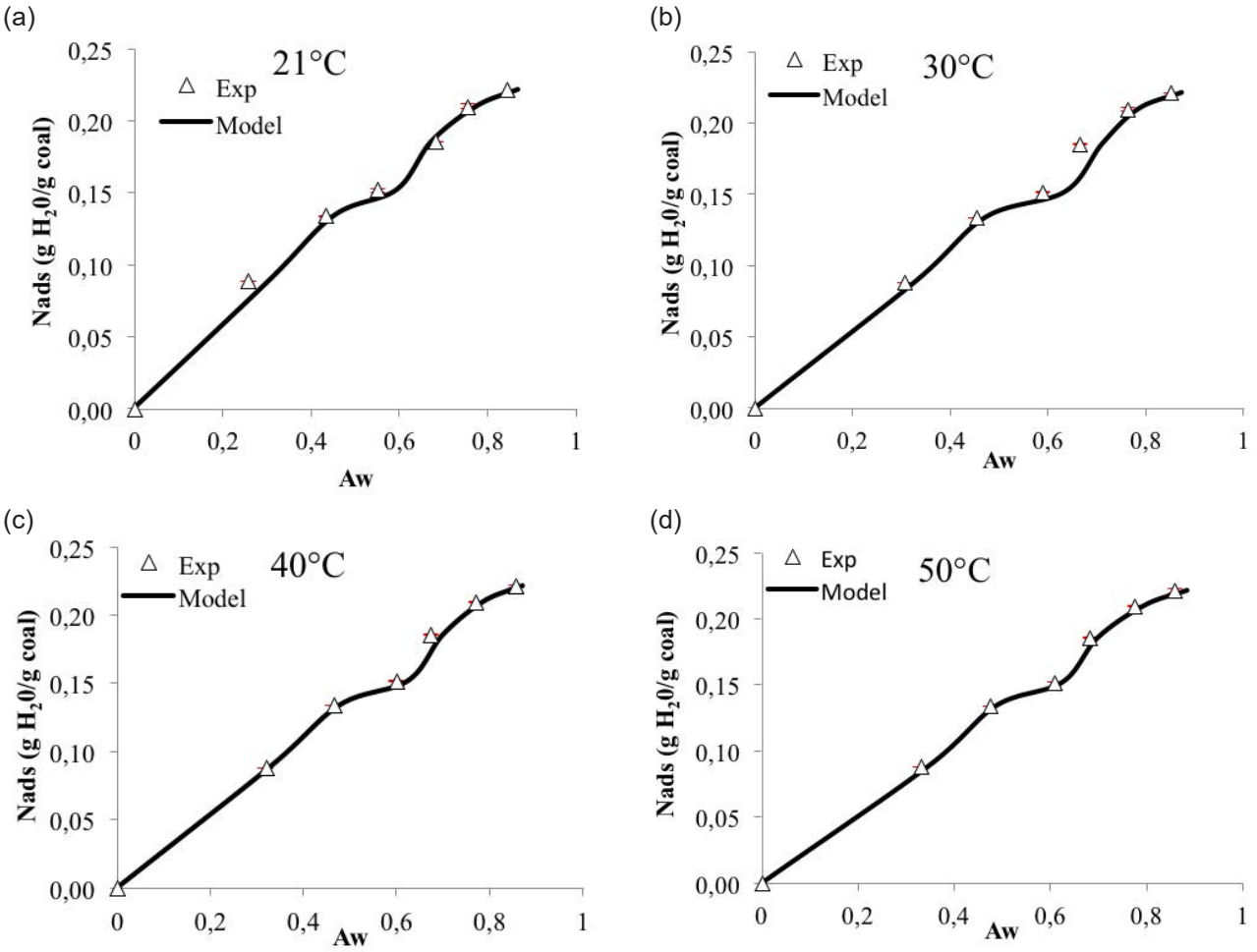

Figure 5. Water adsorption isotherms for coal at (a) 21°C, (b) 30°C, (c) 40°C and (d) 50°C

Table 3. Talu and Meunier model parameters for coal at all of the evaluated temperatures

Temperature	*H (kPa)*	*K (g/g)*	N_m *(g/g)*	MSRE (%)
21	18.5	16.9	0.18	7.45
30	82.5	14.9	0.16	8.12
40	140	14.4	0.15	7.15
50	215	13.5	0.14	4.25

Assuming an ideal gas case, for a constant value of N_{ads} eq. 4 can be simplified to eq. 5 [32]:

$$\left(\frac{\partial \ln P}{\partial\left(\frac{1}{T}\right)}\right)_{Nads} = -Q_{isos}/R \qquad (5)$$

From this equation, the isosteric heat can be calculated by determining the slope of the best fit line when ln(*P*) is plotted against *1/ T* [14, 18].

Figure 6 shows the isosteric heat of adsorption of water onto coal. *Qisos* decreases very slightly as function of *Nads* and remains nearly constant at approximately 600 Cal/g. This value is markedly lower than the isosteric heat for the virgin coal. It is suggested that the isosteric heat varies with water loadings to reveal lower heterogeneity energy of the adsorbent. This is because the high-energy points located on the coal surface reduce their energy intensity, then reducing their affinity to water.

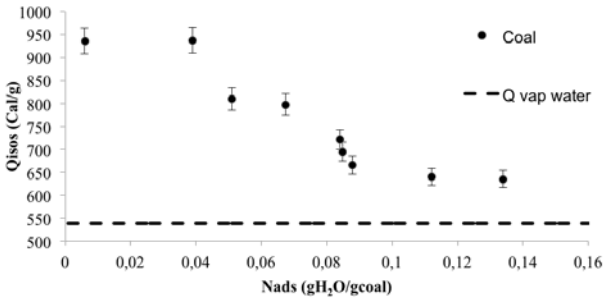

Figure 6. Isosteric heat of adsorption of water onto coal.

This result shows that the decrease very slightly in the energy heterogeneity of the adsorbent is because *Qisos* decreases as the amount of water adsorbed increases. This indicates that the coal surface presents highly energetic and closely related sites for polar compounds, such as water. This information is in agreement with the adsorption equilibrium in which a smaller amount is adsorbed onto the coal sample; therefore, a lower amount of energy is required to desorb the moisture. Figure 6 shows that the amount of energy required for the sample to dry to the desired

Table 4. Net heating value of coal impregnated with different concentrations of glycerol.

MATERIAL	HHV (Cal/g)	NHV (Cal/g)	NHV without the effect of glycerol (Cal/g)
Coal	5194 ± 77.91	4504 ± 67.56	4505 ± 67.56

moisture content is known. These data are important for the design of industrial scale dryers.

The Gibbs free energy of adsorption is a criterion that defines the feasibility and spontaneity of adsorption [13, 35]. The behavior, described by the adsorbed phase, is the same as the condensed phase. This is also known as the condensation approach and can be calculated using eq. 6 [13, 35].

$$\Delta G_0 = A = RTLn\left(\frac{P^0}{P}\right) \quad (6)$$

where, *A(Cal/g)* is the potential for molar adsorption, and *T(K)* and *P(KPa)* are the equilibrium temperature and pressure, respectively. The Gibbs free energy is calculated at a standard pressure "P^o".

Figure 7 shows the change in Gibbs free energy is a function of the adsorbed amount of water on selected samples. For all systems, the Gibbs free energy increases from a negative value to zero. This result demonstrates the thermodynamic consistency of the experimental data and confirms that the reaction is energetically spontaneous and heterogeneous. The data also show that the system is in agreement with the trends of isosteric heat, as reported in Figure 6.

More negative values of Gibbs free energy indicate an exothermic adsorption process; thus, the water molecules are stronger confined to the coal surface. The Gibbs free energy tends toward zero at adsorbed amounts greater than 0.04 g H_2O/g coal (percentages close to 4% moisture). This means that the process is less exothermic and that the strongly adsorbed water molecules are weakly bound to the surface of coal. This is because of the interaction of ambient water molecules with the water molecules already on the coal surface. Therefore, to reduce the moisture content of the treated sample from 10% to 4%, a small amount of energy is required to vaporize the water.

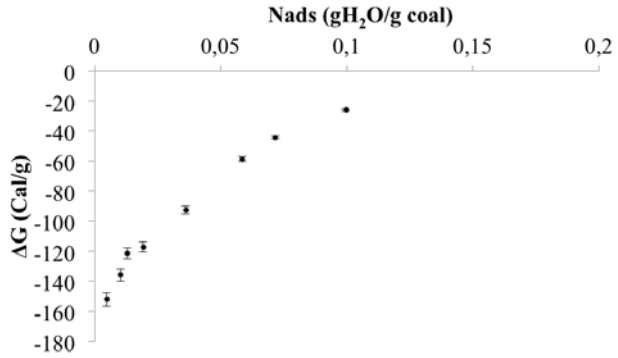

Figure 7. Relationship of Gibbs free energy and the adsorbed amount of water for coal.

3.4 Quality of coal

The heat of combustion of a fuel is commonly referred to as the higher heating value (HHV) or the caloric value. It is defined as the amount of heat released when a unit amount of the fuel is completely combusted. The heating value is a unique characteristic of each type of fuel. The lower heating value (LHV) is similarly defined, except that any water from combustion products is not condensed and remains as vapor. Thus, the LHV does not include the heat of vaporization of the produced water [31]. The relationship between the HHV and the LHV can be expressed as follows [11]:

$$NHV = HHV - Hv \quad (7)$$

For solid fuels (i.e., coal), it is typically expressed as follows [11]:

$$NHV = HHV - 10.55(W + 9Hg) \quad (8)$$

where:

H_v (Cal/g) is the vaporization heat, *NHV* (Cal/g) is the net heating value of coal, *HHV* (Cal/g) is the high heating value of coal in Cal/g, *W* (wt%) is the water amount in coal and *Hg* (wt%) hydrogen in coal.

Table 4 lists the estimated NHV of coal

4. CONCLUSIONS

The sorption equilibrium of water on a sample of sub-bituminous Colombian coal was obtained at 21, 30, 40 and 50°C through the static adsorption method. The results showed that the water uptake increased as the vapor pressure increased and decreases as temperature increases, with maximum water adsorbed was found at 21°C. The Talu and Meunier model was used to fit the adsorption isotherms, and the mean square root error (MSRE%) was lower than 10%. Additionally, the Gibbs free energy was found to have negative values, which corroborates the spontaneous adsorption process.

The thermodynamic properties in caloric value indicate lower costs per unit of energy and decreased transport costs compared with untreated coal.

5. ACKNOWLEDGMENTS

The authors acknowledge The Universidad Nacional de Colombia for logistical and financial support and ARGOS S.A.

REFERENCES

[1] Talu, O. and F. Meunier, Adsorption of associating molecules in micropores and application to water on carbon. AIChE journal, 1996. **42**(3): p. 809-819.

[2] Rempel, H., S. Schmidt, and U. Schwarz-Schampera, Reserves, resources and availability of energy resources. Hannover, Bundesanstalt für Geowissenschaften und Rohstoffe (BGR): www. bgr. bund. de, 2009.

[3] Rutledge, D., Hubbert's peak, the coal question, and climate change. Excel Workbook (permission is given to copy this work provided that attribution is given and the following web link is included). Website: http://rutledge. caltech. edu, 2007.

[4] Castro, J., Perspectivas de la demanda energética global.

Petrotecnia, 2011(1): p. 54-70.

[5] Dubinin, M., Inhomogeneous microporous structures of carbonaceous adsorbents. Carbon, 1981. **19**(4): p. 321-324.

[6] Dubinin, M. and V. Serpinsky, Isotherm equation for water vapor adsorption by microporous carbonaceous adsorbents. Carbon, 1981. **19**(5): p. 402-403.

[7] Bowes, P., Self-heating: evaluating and controlling the hazards. 1984: Department of the Environment, Building Research Establishment.

[8] Carras, J.N. and B.C. Young, Self-heating of coal and related materials: models, application and test methods. Progress in Energy and Combustion Science, 1994. **20**(1): p. 1-15.

[9] Nalbandian, H., Propensity of coal to self-heat. 2010: IEA Clean Coal Centre London.

[10] Kaymakci, E. and V. Didari, Relations between coal properties and spontaneous combustion parameters. Turkish Journal of Engineering and Environmental Sciences, 2002. **26**(1): p. 59-64.

[11] Gossman, D., Net Heating Values versus High Heating Values. GCI tech notes, 2011. **16**(1): p. 1.

[12] Brunauer, S., P.H. Emmett, and E. Teller, Adsorption of gases in multimolecular layers. Journal of the American chemical society, 1938. **60**(2): p. 309-319.

[13] Cortés, F., et al., Water adsorption on zeolite 13X: comparison of the two methods based on mass spectrometry and thermogravimetry. Adsorption, 2010. **16**(3): p. 141-146.

[14] Rouguerol, F., J. Rouguerol, and K. Sing, Adsorption by Powders and Porous Solid; Principles, Methodology and Applications. 1999, Academic Press, San Diego.

[15] Franco, C., et al., Water Remediation Based on Oil Adsorption Using Nanosilicates Functionalized with a Petroleum Vacuum Residue. Adsorption Science & Technology, 2014. **32**(2-3): p. 197-208.

[16] Franco, C.A., et al., Adsorption and Subsequent Oxidation of Colombian Asphaltenes onto Nickel and/or Palladium Oxide Supported on Fumed Silica Nanoparticles. Energy & Fuels, 2013. **27**(12): p. 7336-7347.

[17] Franco, C.A., N.N. Nassar, and F.B. Cortés, Removal of oil from oil-in-saltwater emulsions by adsorption onto nano-alumina functionalized with petroleum vacuum residue. Journal of colloid and interface science, 2014. **433**: p. 58-67.

[18] Comaposada, J., P. Gou, and J. Arnau, The effect of sodium chloride content and temperature on pork meat isotherms. Meat Science, 2000. **55**(3): p. 291-295.

[19] Vos, P.T. and T.P. Labuza, Technique for measurement of water activity in the high aw range. Journal of agricultural and food chemistry, 1974. **22**(2): p. 326-327.

[20] Coleman, R. Irreversible drying of carbonaceous fuels such as low-rank coals. in Fuel and Energy Abstracts. 1996. Elsevier.

[21] Cortés, F.B., V. López, and B.A. Rojano, Sorption properties of Cape gooseberry (Physalis peruviana L.). International Journal of Food Engineering, 2012. **8**(1).

[22] Davy, R., et al., Residual moisture reduction of coarse coal using air purging. 2. Pilot scale studies. Minerals engineering, 2001. **14**(6): p. 671-680.

[23] Nishino, J., Adsorption of water vapor and carbon dioxide at carboxylic functional groups on the surface of coal. Fuel, 2001. **80**(5): p. 757-764.

[24] OMAÑA, M., et al., Isotermas de sorción de agua en residuos de extracción de jugo de naranja. Biotecnología en el Sector Agropecuario y Agroindustrial, 2010. **8**(1): p. 61-67.

[25] Zapata, K., B.A. Rojano, and F.B. Cortés, Effect of Relative Humidity on the Antioxidant Activity of Spray-Dried Banana Passion Fruit (Passiflora Mollisima Baley)-Coated Pulp: Measurement of the Thermodynamic Properties of Sorption. Chemical Engineering Communications, 2015. **202**(3): p. 269-278.

[26] Allardice, D., et al., The characterisation of different forms of water in low rank coals and some hydrothermally dried products. Fuel, 2003. **82**(6): p. 661-667.

[27] Charrière, D. and P. Behra, Water sorption on coals. Journal of colloid and interface science, 2010. **344**(2): p. 460-467.

[28] Chen, X.D., A new water sorption equilibrium isotherm model. Food research international, 1997. **30**(10): p. 755-759.

[29] Karthikeyan, M., et al., Factors affecting quality of dried low-rank coals. Drying Technology, 2007. **25**(10): p. 1601-1611.

[30] Marchessault, R., Application of infra-red spectroscopy to cellulose and wood polysaccharides. Pure and Applied Chemistry, 1962. **5**(1-2): p. 107-130.

[31] McCain, W.D., The properties of petroleum fluids. 1990: PennWell Books.

[32] Shigehisa, T., T. Inoue, and H. Kumagai, Mathematical model of water sorption isotherms of UBC. Fuel Processing Technology, 2015. **131**: p. 133-141.

[33] Sing, K.S., Reporting physisorption data for gas/solid systems with special reference to the determination of surface area and porosity (Recommendations 1984). Pure and applied chemistry, 1985. **57**(4): p. 603-619.

[34] Peinter, P., M. Starsinic, and M. Coleman, Determination of functional groups in coal by fourier transform interferometry, fourier transform infrared spectroscopy. Academic Press, New York, 1985. **4**: p. 169.

[35] Soares, J.L., Desenvolvimento de novos adsorventes e processos híbridos em reforma catalítica por vapor de água. 2003.

[36] Cortes, F.B., B. Rojano, and F. Chejne Janna, Advantages and thermodynamic limitations of the experimental sorption isosteric method. Dyna, 2013. **80**(182): p. 155-162.

[37] Seifert, J. and G. Emig, Mikrostrukturuntersuchungen an porösen Feststoffen durch Physisorptionsmessungen. Chemie Ingenieur Technik, 1987. **59**(6): p. 475-484.

Determinación de parámetros cinéticos para la pirólisis rápida de aserrín de pino pátula

Arango-Muñoz, Melisa[1], Arenas-Castiblanco, Erika[1], Cortes-Correa Farid[2]

[1] *Universidad Pontificia Bolivariana. melisa.arango@upb.edu.co - erika.arenas@upb.edu.co*

[2] *Universidad Nacional de Colombia Sede Medellín. fbcortes@unal.edu.co*

Resumen

Frente a la crisis energético-ambiental en que nos encontramos en la actualidad, se presenta la necesidad de evaluar nuevas fuentes energéticas que suplan la dependencia del petróleo y los combustibles fósiles, es por esto que el estudio de pirólisis ha ganado gran importancia hoy, esta es la primera etapa en cualquier proceso de gasificación o combustión para las nuevas fuentes. En este estudio se llevó a cabo la determinación de la cinética química de la pirólisis rápida de aserrín de pino pátula por medio de un estudio termogravimétrico. Para este, primero se preparó la muestra de aserrín, garantizando un tamaño de partícula de 600μm, además se lleva a cabo un secado superficial en un horno a 110ºC. Una vez ajustado el tamaño de partícula y humedad de la muestra se realizó el análisis termogravimétrico en un sistema TGA para llevar a cabo una degradación másica gradual, en la que se variaron tres rampas de calentamiento de 5ºC/min, 20ºCmin y 50ºC/min. Fijando el flujo de nitrógeno en 60mL/min. Por último, para obtener los parámetros de energía de activación (E) y factor exponencial (A) se aplicaron dos modelos cinéticos no isotérmicos, el diferencial de Friedman y el integral de Coats y Redfern.

Palabras clave: Pirólisis rápida, cinética, aserrín de pino pátula, análisis termogravimétrico, TGA.

Introducción

En la actualidad el ser humano consume 500 QBTU de energía, y aproximadamente un 92% de esta, viene de fuentes no renovables, como petróleo, carbón, gas natural y nuclear. Debido a que solo un 8% de la energía consumida por el hombre proviene de fuentes renovables, la sustitución de los combustibles derivados del petróleo por biomasas de origen vegetal o residuos industriales cobra gran importancia hoy en día como alternativa para disminuir la cantidad de emisiones de CO_2, SO_X, NO_X y material particulado producidas durante procesos de producción de energía [1].

La biomasa puede ser pirolisada o gasificada alternativamente produciendo un combustible líquido o gaseoso como metano, hidrógeno o monóxido de carbono. La pirólisis rápida es un proceso termoquímico que se realiza a alta temperatura, en el cual la biomasa es calentada rápidamente en ausencia de oxígeno. Como resultado ésta se descompone para generar vapores, gases y carbonizado. Los vapores generados son posteriormente enfriados y condensados para obtener un bio-oil o combustible líquido. Este es una mezcla miscible de orgánicos polares (entre 75- 80%) y agua (20-25%). Éste tiene muchas aplicaciones en el campo de la energía y los combustibles, ya que puede ser usado como precursor de otros compuestos químicos y ha sido probado para aplicaciones en diferentes motores [2-4].

Este proceso es preferible a una pirólisis lenta en cuanto a la alta producción de líquidos, es un proceso avanzado controlado para obtener altos rendimientos. Diferentes estudios han mostrado que se obtienen valores máximos de rendimientos para liquido a altas tasas de calentamiento entre 30 y 150ºC/min, temperaturas de reacción alrededor de 500ºC y con bajos tiempos de residencia de vapor para minimizar reacciones secundarias [4,5].

La pirólisis siempre es el primer paso en los procesos de combustión y gasificación, seguido de una oxidación total o parcial de los productos primarios [6]. Por lo tanto para estandarizar procesos a escala industrial para la producción de biocombustibles a partir de estas fuentes renovables, y lograr desplazar los combustibles obtenidos de materiales fósiles, se debe conocer a fondo lo que ocurre en el proceso. Uno de los aspectos principales a conocer es la cinética química, porque esta será base fundamental para el diseño de la zona de reacción del proceso.

El análisis termogravimétrico (TGA) es un método bien establecido en la determinación de las características de pérdida másica y su cinética de reacción asociada. Este tipo de análisis implica la degradación térmica de la muestra en una atmósfera inerte con registro simultáneo de pérdida másica de la muestra a medida que aumenta la temperatura a una velocidad constante [7]. Este tipo de análisis es de gran importancia a nivel industrial, las ecuaciones cinéticas determinan las condiciones del proceso como temperaturas, cantidades y concentraciones de reactivos, con las que haciendo un análisis más a fondo se llega a escalar plantas pirolíticas para la obtención masiva de bio-oil reduciendo a nivel mundial emisiones de gases invernadero y la dependencia de derivados del petróleo.

1. Metodología

1.1 Preparación de la muestra

Las partículas de aserrín de pino pátula se dispusieron en bandejas en un lugar seco a temperatura ambiente (24 a 26ºC) durante 1 día para eliminar la humedad superficial con que llega la muestra. Una vez seca se realizó un tamizado con el fin de obtener una muestra con un tamaño de 600μm. Finalmente la biomasa se llevó a un horno a 110ºC monitoreando hasta obtener peso constante.

1.2 Método pirólisis aserrín

La muestra seca y con un tamaño uniforme se llevó un analizador termogravimétrico TA Instrument TGA-Q50 para realizar una degradación másica gradual a las diferentes rampas de calentamiento. Por restricciones del TGA el flujo de Nitrógeno (N_2) alimentado a la termobalanza es de 60mL/min. La muestra sólida de 5mg aproximadamente fue dispuesta en una canasta de aluminio con base redonda para cada ensayo. La termobalanza equipada con un horno eléctrico puedo operar hasta

1000ºC con un controlador de temperatura. Dentro del horno se encuentra un termopar cerca de la canasta de aluminio para monitorear la temperatura durante el experimento. La pérdida másica, temperatura y tiempo son las variables monitoreadas continuamente.

Inicialmente la muestra fue llevada hasta 120ºC a 5ºC/min y se mantuvo en esta temperatura por 12 minutos con el fin de eliminar los rastros de agua presentes en el aserrín. Posteriormente se elevó la temperatura hasta 800ºC a la misma velocidad y se mantuvo en 800ºC durante 30 minutos más.Este proceso se realizó del mismo modo a velocidades de 20ºC/min y 50ºC/min. El gas de arrastre empleado es nitrógeno para garantizar características inertes en el proceso a 60mL/min.

1.3 Modelos Cinéticos

Para evaluar los datos obtenidos de degradación másica a diferentes rampas de calentamiento, se modeló la cinética química de la reacción de pirolisis por dos métodos no isotérmicos diferentes, uno diferencial y otro integral.

Método diferencial de Friedman

Éste es el método más general, se basa en la comparación de las velocidades de pérdida de peso ($d\alpha/dT$) para un pérdida de peso fraccional, usando diferentes velocidades de calentamiento. Este método emplea la siguiente ecuación diferencial para diferentes velocidades de calentamiento β. Teniendo en cuenta que $\beta=dT/dt$:

$$\frac{d\alpha}{dT} = \frac{A}{\beta} e^{-Ea/RT} f(\alpha) \qquad (1)$$

A esta expresión se le aplica una linealización y teniendo en cuenta la ecuación 6 se obtiene:

$$\ln\left(\frac{d\alpha}{dT}\right) = \ln\frac{A}{\beta} - \frac{Ea}{RT} + \ln[(1-\alpha)^n] \qquad (2)$$

En este método es necesario trabajar en un rango de grados de avance a en el que el ajuste lineal sea adecuado. De tal manera que para obtener un buen ajuste lineal, se analiza en un gráfico de (da/dT) vs a el intervalo anterior al punto máximo de la campana donde el comportamiento es lineal.

A partir de la expresión 10 se puede determinar el valor de la energía de activación aparente para cada velocidad considerada a partir de la pendiente del gráfico de ln ($d\alpha/dT$) vs 1/T. Una vez calculado el valor de Ea, es posible determinar el orden de reacción y el factor preexponencial representando los valores de $Ln(d\alpha/dT)+Ea/R\cdot T$ frente a $Ln(1-\alpha)$. Este ajuste debe dar una línea recta cuya pendiente es el orden de reacción y cuya ordenada en el origen es el $Ln(A/\beta)$ [8].

Método Integral de Coats y Redferm

La ecuación básica de cinética es la siguiente:

$$\frac{d\alpha}{dt} = kf(\alpha) \qquad (3)$$

Donde α es la conversión de la biomasa, como se muestra:

$$\alpha = \frac{m_o - m}{m_o - m_\infty} \qquad (4)$$

m_o representa el peso inicial de la muestra, m es el peso de la muestra a un tiempo t, y m_∞ es el peso final de la muestra.

Por otro lado la constante de reacción, k está dada por la expresión de Arrhenius:

$$k = A\exp\left(-\frac{E}{RT}\right) \qquad (5)$$

Donde A es el factor preexponencial (min^{-1}); E es la energía de activación aparente (kJ/mol); T es la temperatura de reacción (K); R es la constante de gases igual a $8.314x10^{-3}$ kJ/mol K.

La Temperatura de reacción puede ser expresada como:

$$T = T_o + \beta t \qquad (6)$$

Donde T_o es la temperatura inicial (K) y β es la velocidad de calentamiento (K/min).

Reemplazando las expresiones, la ecuación 1 queda como:

$$\frac{d\alpha}{dT} = \frac{A}{\beta} f(\alpha) exp\left(-\frac{E}{RT}\right) \qquad (7)$$

$f(\alpha)$ se representa como:

$$f(\alpha) = (1-\alpha)^n \qquad (8)$$

Donde n es el orden de reacción. Para este proceso se toma un valor de n=1, basado en estudios anteriores donde una aproximación de primer orden de reacción es válida para pirólisis de biomasas lignocelulósicas [7].

Una combinación de las ecuaciones 5 y 6 y posterior integración se convierte en:

$$\int_0^\alpha \frac{d\alpha}{(1-\alpha)^n T^2} = \frac{AR}{\beta E}\left[exp\left(-\frac{E}{RT}\right) - exp\left(-\frac{E}{RT_o}\right)\right] \qquad (9)$$

Pero el término $\frac{E}{RT_o} \approx 0$ de la ecuación 7 puede despreciarse, reduciéndose a:

$$\ln\int_0^\alpha \frac{d\alpha}{(1-\alpha)^n T^2} = \ln\frac{AR}{\beta E} - \frac{E}{RT} \qquad (10)$$

El lado izquierdo de la ecuación se puede graficar contra 1/T de donde la pendiente de la línea recta es corresponde a la Energía de activación aparente (E) [7].

Resultados y Discusión

Las curvas TGA y DTG para las muestras bajo atmósfera inerte son dadas en las Figuras 1-3. y son usadas para determinar las características térmicas del aserrín para cada una de las velocidades de calentamiento (β).

A partir de estas curvas se ubican las fases térmicas para cada una de las β. Para 5ºC/min, se observa el inicio de la pirólisis en 250ºC y termina en 370ºC,

para 20ºC/min inicia en 250ºC y termina en 400ºC, por último para 50ºC/min se observa la iniciación de la fase pirolítica en 250ºC y termina en 420ºC aproximadamente. Si se sobreponen los gráficos se puede observar el desplazamiento esperado de las curvas hacia la derecha a medida que aumenta la velocidad de calentamiento. Teniendo en cuenta que la biomasa empleada contiene principalmente celulosa, hemicelulosa y lignina se ha encontrado que la celulosa se descompone entre 277 y 427 ºC, la hemicelulosa alrededor de 197 y 327 ºC y la lignina entre 277 y 527 ºC, se observó que la descomposición del aserrín después de 400 ºC avanza más lentamente debido a las características de la lignina [5].

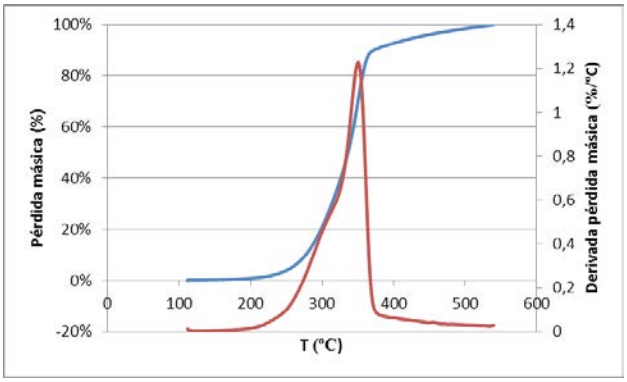

Figura 1. Curvas TGA y DTG para pirólisis de aserrín a 5ºC/min

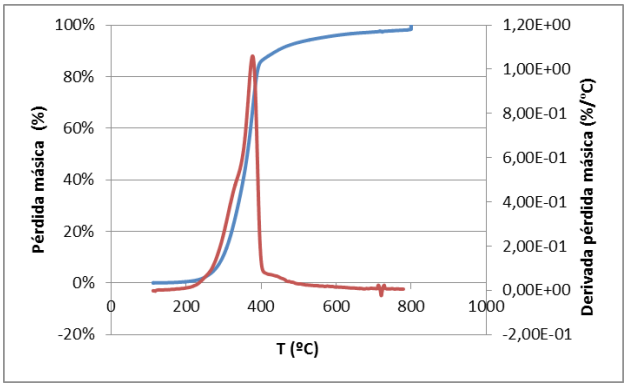

Figura 2. Curvas TGA y DTG para pirólisis de aserrín a 20ºC/min.

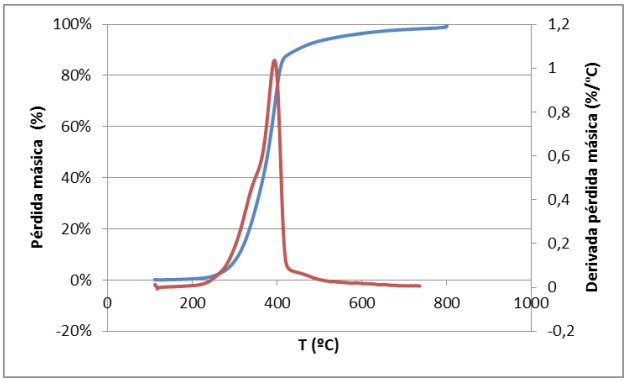

Figura 3. Curvas TGA y DTG para pirólisis de aserrín a 50ºC/min.

Para esta biomasa se presenta un solo pico de máxima descomposición térmica en los rangos entre 200-400ºC el cual es atribuido a la descomposición de la celulosa y la hemicelulosa. Estos picos se ubican en 350ºC, 375ºC y 392ºC respectivamente para cada b. Con el aumento de la β se observa un desplazamiento hacia la derecha de los picos de máxima descomposición; este ocurre debido a que hay mayores tiempos de reacción a temperaturas mayores, además la máxima velocidad de descomposición tiende a incrementar a mayores velocidades de calentamiento porque se provee una mayor energía térmica que facilita la transferencia de calor alrededor y dentro de las muestras [5].

Los análisis de los gráficos TGA fueron usados para determinar los parámetros cinéticos del aserrín de pino pátula, tales como la energía de activación aparente (Ea) y el factor preexponencial (A) con el método diferencial de Friedman. Basados en la ecuación 2 la energía de activación Ea se determina por la relación entre ln(dα/dT) y 1/T. Es importante resaltar que antes de llevar a cabo este método, se debe ubicar el rango de a en el que se hace válido este modelo como se explicó anteriormente, la figura 4 muestra para una velocidad de 5ºC/min, la ubicación de dicho rango y este procedimiento se realiza del mismo modo para cada una de las curvas a las diferentes β.

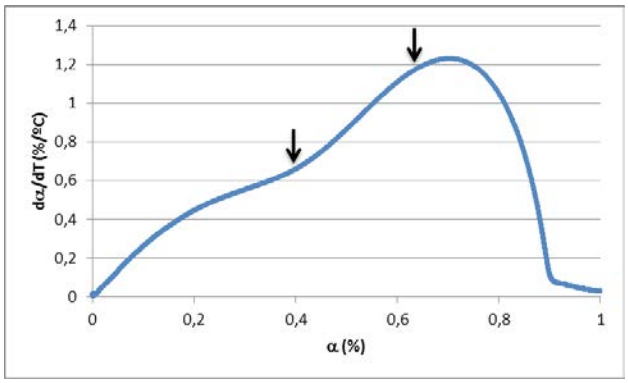

Figura 4. Ubicación rango α válido para el método Friedman para 5ºC/min.

Una vez ubicado el rango se procede a graficar ln(dα/dT) y 1/T como se muestra en la Figura 5, resultando una línea recta de la cual la pendiente corresponde a -Ea/R, y a partir de esta se determinan los valores de Ea para cada β. Estos valores se encuentran consignados en la Tabla 1. Una vez encontrados los valores de Ea se determinan los órdenes de reacción (n) y factor preexponencial (A) a partir de la relación entre Ln(dα/dT)+Ea/R·T frente a Ln(1-α). Este ajuste debe dar una línea recta cuya pendiente es el orden de reacción y cuya ordenada en el origen es el Ln(A/β). Así se encuentran los valores de n y A reportados en la Tabla 1. Estos procedimientos se realizan de igual manera para cada una de las velocidades de calentamiento.

Posterior a este método, se llevó a cabo el método integral de Coats y Redfern. Se realizó una suposición de orden de reacción n=1, válida para esta biomasa según los resultados del método anterior, debido a que los valores de n para cada una de las velocidades varían entre 1.19 y 1.34 como se observa en la Tabla 1. Con esta suposición el resultante de la integración del lado izquierdo de la ecuación 10 queda $\ln\left(\frac{-ln(1-\alpha)}{T^2}\right)$ y este el que se grafica con respecto a 1/T, línea recta de la cual su pendiente corresponde a –Ea/R. Es así como se determinan los valores de Ea para cada una de las velocidades de calentamiento y son reportados en la Tabla 2.

Autores como Joaquin Reina et al, y Nancy Acelas et

al, trabajaron con biomasas lignocelulósicas, como maderas y residuos madereros obteniendo valores cinéticos de una magnitud similar a los obtenidos en el presente estudio, variando entre 127kJ/mol y 157kJ/mol respectivamente entre los autores. Además los valores de orden de reacción obtenidos son esperados para este tipo de biomasa según lo reportado en la literatura. [5,9]

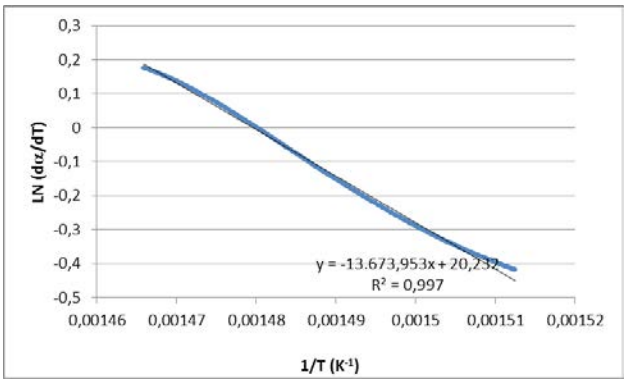

Figura 5. Aplicación de la Ecuación 2 a 5ºC/min.

Tabla 1. Resumen resultados método Friedman con los respectivos coeficientes de correlación de tendencia lineal.

β (ºC/min)	5	20	50
Ea (kJ/mol)	113.685	148.594	291.900
n	1.198	1.336	1.198
A	1.839	6.356	17.063
r^2_1	0.996	0.990	0.996
r^2_2	0.979	0.9949	0.9839

Donde r^2_1 corresponde a linealización respectiva para la determinación de Ea y r^2_2 a la respectiva a la determinación de n y A.

Tabla 2. Resumen resultados método Coats-Redfern con los respectivos coeficientes de correlación de tendencia lineal.

β (ºC/min)	5	20	50
Ea (kJ/mol)	105.009	163.802	270.5872
r^2	0.995	0.998	0.999

Conclusiones

Los análisis termogravimétricos para la pirólisis del aserrín de pino pátula fueron utilizados para determinar los parámetros cinéticos, tales como, energía de activación, orden de reacción y factor pre-exponencial. La energía de activación determinada por el método diferencial estuvo en el rango de 113.68-291.9kJ/mol dependiendo de las velocidades de calentamiento y por el método integral estuvo en el rango de 105-270.59kJ/mol, resultando valores similares en magnitud para ambos métodos y manteniendo una tendencia a aumentar con el incremento de la velocidad de calentamiento.

Los órdenes de reacción obtenidos con el método diferencial son esperados según lo reportado y validan la suposición necesaria para aplicar el método integral.

El aserrín se descompuso en el rango de temperaturas entre 250 y 420 ºC, lo cual sugiere que éste tipo de biomasa contiene mayor cantidad de hemicelulosa y celulosa.

Referencias Bibliográficas

[1] Buelvas, M. (2007). Estado del arte en la producción de Biodiesel. Universidad Nacional de Colombia.

[2] Senneca, O. (2007). Kinetics of pyrolysis, combustion and gasification of three biomass fuels. Fuel processsing technology (88), 87-97.

[3] Brammer, J., Laurer, M., & Bridgwater, A. (2006). Opportunities for biomass-derived “bio-oil” in European geat and power markets. Energy Policy , 2871-2880.

[4] Bridgwater, A., Mejer, D., & Radlein, D. (1999). An overview of fast pyrolysis of biomass. Organic Geochemistry , 1479-1493.

[5] Acelas Soto, N., Ruíz Machado, W., & López López, D. (2010). Deteminación de los parámetros cinéticos en la pirólisis del pino ciprés. Quim. Nova , 33 (7), 1500-1505.

[6] Montoya Arbeláez, J. I. (2013). Pirólisis rápida de Biomasa. Medellín: Universidad Nacional de Colombia.

[7] Singh, S., Wu, C., Williams, P. (2012). Pyrolysis of waste materials using TGA-MS and TGA-FTIR as complementary characterisation techniques. Journal of Analytical and Applied Pyrolysis (94), 99-107.

[8] Fiaco, J., López, J., Arrieta, M. (2013). Evaluación de modelos de degradación de polímeros basados en la lignina. Universidad politécnica de Valencia. Disponible en la web: https://riunet.upv.es/

[9] Reina, J., Velo, E., Puigjaner, Luis. (1998). Thermogravimetric study of the pyrolysis of waste Wood. Thermochimica Acta (320), 161-167.

Activation process of spherical and fibrous carbon precursors for Gas phase adsorption of volatile organic compounds

A. J. Romero Anaya
PhD Instituto Colombiano del Petróleo (ICP) Ecopetrol S.A.
** Corresponding author: aroldo.romero@ecopetrol.com.co*

Objetives and novelty:

Activated carbons (ACs) are amongst the most promising materials in environmental applications. Hence, new applications are emerging constantly, which imply that the world consumption of these materials is steadily increasing. Among the different methods employed in the preparation of new carbon materials, the interest on the hydrothermal treatment for the preparation of spherical materials can be remarked due to the advantages that the spherical carbons have in comparison with granular activated carbons or powdered activated carbons. The lignocellulosic and carbohydrate materials are interesting precursors for the preparation of spherical carbons by hydrothermal treatment due to their low cost and for environmental concerns.

Additionally, although several authors have reported that hydrothermal treatment is a method to get a wide range of spherical carbon materials with controlled and functionalized structures (or nanostructures) from cheap and abundant precursors, few studies have analyzed the porosity development of the spherical carbons once the spheres have been prepared, and in each paper only one activation method is studied.

In this sense, this PhD Thesis has focused on the study of the preparation of spherical carbons and spherical activated carbons (SAC) by hydrothermal treatment of two natural bio-fibre precursors (banana pseudostem and coconut fibre matting) using three carbohydrates with different structure, a monosaccharide (glucose), a disaccharide (saccharose) and a polysaccharide (cellulose). Afterwards, the activation of these materials by several techniques, keeping the spherical morphology, has been deeply investigated. Regarding the hydrothermal preparation of spherical carbons, the effect of different variables (treatment time, treatment temperature, type of precursor and concentration of carbohydrate) on the spherical carbons formation and their properties have been analyzed.

For the development of the adsorption capacity of these spherical carbons, different activation methods have been analyzed (chemical activation with H_3PO_4, NaOH or KOH or physical activation with CO_2). The effect of some variables such as the precursor, the activation method, the activating agent/precursor ratio (in chemical activation) or the activation time (in physical activation) on the textural properties of the prepared spherical activated carbons has been deeply studied. Also, for comparison purposes a commercial spherical carbon (GE) and a commercial spherical activated carbon (BAC) have been selected as precursors to prepare spherical activated carbons through physical activation with CO_2 and/or steam.

All the prepared samples have been characterized by SEM, thermogravimetry, N_2 adsorption at -196 ºC and CO_2 adsorption at 0 ºC. The pore size distributions were obtained applying the nonlocal density functional theory (NLDFT) to the N_2 adsorption data at -196 ºC. The characterization of the surface oxygen chemistry of all the samples has been performed by temperature-programmed desorption (TPD). The prepared materials have been employed in the adsorption of volatile organic compounds (VOCs): a non-polar volatile organic compound (toluene) at low concentration, a polar volatile organic compound (ethanol) at low relative pressures (lower than 0.01) and relative pressure near unity, and in gasoline vapors in conditions similar to those in vehicle tanks.

Results:

Spherical activated carbons have been prepared from spherical carbons that had been previously obtained by hydrothermal treatment of glucose and saccharose and, also, from a commercial spherical carbon (GE) and a commercial spherical activated carbon (BAC). H_3PO_4 , KOH, NaOH, CO_2 and steam activation have successfully developed the textural properties in these materials, maintaining the spherical morphology and reaching surface areas higher than 3100 m^2/g, micropore volumes up to 1.21 cm^3/g, narrow micropore volumes up to 0.76 cm^3/g or mesopore volumes up to 0.57 cm^3/g. Besides their textural properties, the prepared SACs must be remarked in terms of variability of their surface oxygen chemistry content, strongly dependent on the preparation method selected, which makes these materials very interesting for the adsorption of polar or non-polar VOCs adsorption at different concentration ranges. The SACs prepared have high microporosity and low surface oxygen groups content, which make them interesting for their application for nonpolar VOCs adsorption at low concentrations. In this sense, SACs with high adsorption capacity have been prepared, leading to gravimetric adsorption capacities as high as 70 g toluene/100 g, higher than those achieved with the commercial WVA1100 AC. Also, considering the high gravimetric adsorption capacities and the high bed densities for these materials, especially in the case of the SACs prepared from commercial precursor, the volumetric adsorption capacities achieved are quite high, up to 236 g of toluene/L AC, for the SACs obtained from GE, much higher than that obtained with the commercial WVA1100 AC (see Fig. 1). Thus, besides the textural properties, high bed densities are required for getting high volumetric adsorption capacities.

The adsorption results at low ethanol relative pressures on five spherical activated carbons (from BAC), which have similar textural properties but different surface oxygen chemistry, show that surface chemistry has an important influence on the ethanol adsorption capacity. This influence is not due to the total oxygen content of the samples, but especially to the kind/nature of these oxygen functional groups.

Thus, the presence of carboxyl and anhydride groups, generated by HNO_3 oxidation, favours ethanol adsorption at low concentration, whereas the presence of phenols and carbonyls, generated by air oxidation, is negative. On the contrary, the analysis performed at high ethanol concentration

shows that the adsorption capacities depend only on the porosity, and not on the surface chemistry of the ACs, which is confirmed by the 14 samples selected and studied. In particular, the total micropore volume governs ethanol adsorption in these conditions, as it can be seen in Fig. 2.

The activated carbons prepared from lignocellulosic precursors through H_3PO_4 activation have developed high apparent surface areas, up to 2500 m^2 g^{-1}, high micropore volumes (above 1.00 cm^3 g^{-1}) and high mesopore volumes (1.41 cm^3 g^{-1}). Most of the activated carbons obtained in this study perform very well for adsorbing gasoline vapours, being their performance linearly related to their micro+mesoporosity development. Some of the samples prepared are comparable, or even better, to a commercial activated carbon currently used in gasoline automobiles for evaporative emissions control. To confirm the importance of the mesopores, the sample microporosity has been minimised filling it with n-nonane. Fig. 3 confirms the dependence of the gasoline vapours adsorption with the mesopore volume of the samples (after microporosity has been filled). Additionally, our comparative study shows that the ACs prepared perform very well, even better than WVA1100, a well known commercial activated carbon used to control automobile hydrocarbons emissions.

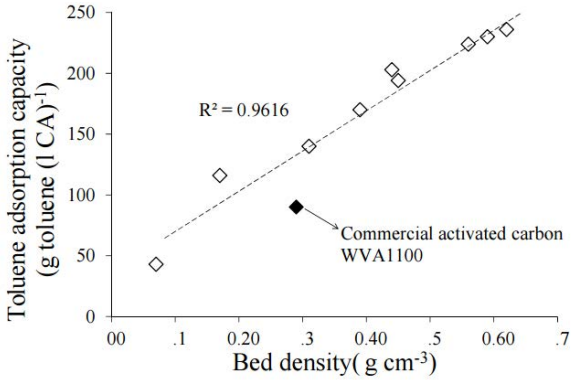

Fig 1. Gravimetric toluene adsorption capacity vs bed density.

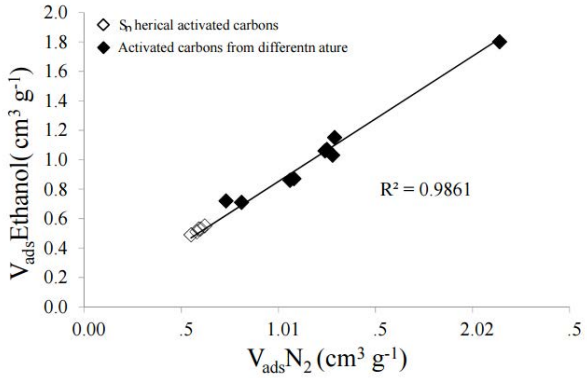

Fig 2. Volumes of N_2 vs ethanol adsorbed (asliquids) at P/Po = 0.95

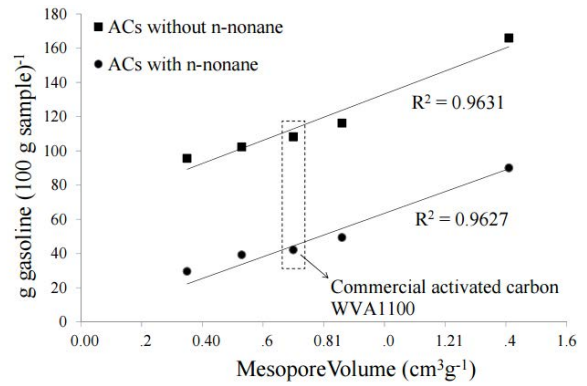

Fig 3. Evaporative gasoline test. Relationship between gasoline uptake and mesopore volume.

Conclusions:

In this PhD Thesis many activated carbons and spherical activated carbons have been prepared with a wide range of surface areas, micropore volumes and mesopore volumes, and they have been applied to the adsorption of polar and non- polar volatile organic compound at low and high relative pressures. At low relative pressures it has been confirmed that spherical activated carbons with low oxygen groups contents and high narrow micropore volumes lead to high toluene adsorption capacity.

Besides the high micropore volumes in the spherical activated carbons, the high bed densities of these materials have allowed to achieve high volumetric adsorption capacities. The adsorption of ethanol at low relative pressures is favored by oxygen groups, especially by the presence of carboxyl and anhydride groups generated by HNO_3 oxidation, whereas at relative pressures near unity porosity controls ethanol adsorption capacity. Finally, gasoline vapor adsorption has been proved to be controlled by the mesoporosity of the activated carbons. The ACs prepared in this Thesis present higher gasoline adsorption capacity than a commercial activated carbon especially designed and used for this application.

Related Publications

[1] Romero-Anaya AJ, Lillo-Ródenas MA, Linares-Solano. Spherical activated carbons for low concentration toluene adsorption. Carbon 2010; 48:2625-2633.

[2] Romero-Anaya AJ, Molina A, Garcia P, Ruiz-Colorado AA, Linares-Solano A, Salinas-Martínez de Lecea C. Phosphoric acid activation of recalcitrant biomass originated in ethanol production from banana plants. Biomass and Bioenergy 2011; 35:1196-1204.

[3] Romero-Anaya AJ, Lillo-Ródenas MA, Salinas-Martínez de Lecea C, Linares-Solano A. Hydrothermal and conventional H_3PO_4 activation of two natural bio-fibers. Carbon 2012;50(9):3158-69.

[4] Linares-Solano A, Lillo-Ródenas MA, Marco-Lozar JP, Kunowsky M, Romero-Anaya AJ. Utility of Sodium and Potassium Hydroxides for Preparing Superior Quality Activated Carbons. In: Abejundio Calixto Carillo and Delia Analiz Griego Editors. Hydroxides: Synthesis, Types and Applications. NOVA Editors. 2012 3rd Quarter.

[5] Linares-Solano A, Lillo-Ródenas MA, Marco-Lozar JP, Kunowsky M, Romero-Anaya AJ. NaOH and KOH for preparing activated carbons used in energy and environmental applications. International Journal of Energy, Environment and Economics. 2012;20(4);59-91.

[6] Ouzzine M, Romero-Anaya AJ, Lillo-Ródenas MA, LinaresSolano A. Spherical activated carbon as an enhanced support for TiO_2/AC photocatalysts. Carbon 2014;67:104-18.

[7] Romero-Anaya AJ, Ouzzine M, Lillo-Ródenas MA, LinaresSolano A. Spherical carbons: Synthesis, characterization and activation processes. Carbon 2014;68:296-307.

[8] Romero-Anaya AJ, Lillo-Ródenas MA, Linares-Solano A. Activation of a spherical carbon for toluene adsorption at low concentration. Carbon 2014;77:616-626.

[9] Romero-Anaya AJ, Lillo-Ródenas MA, Linares-Solano A. Factors governing the adsorption of ethanol on spherical activated carbons. Carbon 2015;82:240-49.

Full Thesis can be downloaded from:

http://hdl.handle.net/10045/30715

Thesis Review. Covalent functionalization of carbon nanotubes and graphene for catalysis applications

M. Blanco

Presented on 2015. Departamento de Ciencia de los Materiales e Ingeniería Metalúrgica, University of Oviedo. Instituto Nacional del Carbón INCAR-CSIC, P.O. Box 73, 33080 Oviedo, Spain.

Supervisors: R. Menéndez and P. Álvarez.

OBJECTIVES AND NOVELTY

Carbon nanotubes (CNT) and graphene are recently discovered carbon nanomaterials which find application in a great number of fields. Their excellent mechanical, electrical, thermal and chemical properties make them useful for a wide range of new developments which move from electronic devices to drug-delivery systems. In addition, catalytic systems usually employ carbon nanotubes and graphene in any of the stages of the catalytic process.

In this work, the integration of carbon nanotubes and graphenic materials in well-known homogeneous catalytic systems, *i.e.* unsaturated-substrates reduction reactions by means of hydrogen transfer processes catalyzed with iridium N-heterocyclic carbene complexes is studied. The employment of different strategies for the preparation of the supports, the design of the nanostructure functionalization routes with the metallic complexes and the study of the catalytic activity of the final hybrid materials are described. Both types of materials were oxidized with the aim of developing oxygen functional groups which allow nanomaterial functionalization methods to be applied with the organometallic compounds. A special effort was made to accomplish a complete and exhaustive characterization of the involved samples by typical solid characterization techniques.

RESULTS

The treatment of carbon nanotubes using reagents with increased oxidation degree led to a proportional increment in the oxygen functional groups at the surface and at the tips of the nanotubes. Only the strongest oxidizing agent introduced more oxygen functional groups in the CNT. These facts modified the capacity of forming stable suspensions in water and they also modify the adsorption behavior. Thus, in the comparative study of benzene adsorption, employed as an additional characterization technique, the most oxidized CNT exhibited faster kinetics and higher adsorption capacity.

The great amount of oxygen moieties introduced in the most oxidized carbon nanotubes allows the functionalization through their carboxylic groups in order to generate new hybrid materials with supported molecular catalysts. They presented enhanced catalytic activity in the reduction reaction of cyclohexanone to cyclohexanol compared to their corresponding homogeneous systems. Figure 1 shows the possible structure of one of the hybrid systems and the comparison in the catalytic activity of the heterogeneous and homogeneous samples. Moreover, they also present excellent cyclability and air stability, in sharp contrast with their analogous non-supported catalysts.

The synthesis of hybrid catalysts supported on graphene oxide was based in a new functionalization strategy, which consists in the modification of the surface hydroxyl groups employing organic-based connectors. The selectivity of the reaction was checked by the functionalization of the corresponding thermally reduced materials which do not possess carboxylic acids. The later were those which presented the best catalytic activity, superior to the homogeneous systems too. In addition, both hybrid catalysts also presented cyclability and air stability. This new functionalization procedure was also confirmed by obtaining analogous supported iridium catalysts on oxidized and thermally reduced carbon nanotubes, which were more active on the same catalytic process. On Figure 2 is schemed the comparison of both types of carbon nanostructures functionalized under the same strategy.

The study of the local environment of the iridium organometallic complexes anchored on the carbonaceous support revealed a direct bond between the metal and the supports, which affects the catalytic activity of the system (Figure 3). The presence of structural defects in the aromatic lattice was demonstrated to generate catalysts with poor activities. Partially reduced materials based catalysts achieved the best performances. Moreover, the correct type and amount of oxygen functional groups are necessary to obtain a good behavior in order to stablish stabilizing bonds between those groups and the metallic center.

CONCLUSIONS

Different iridium NHC organometallic complexes can be introduced in the surface oxygen functional groups of carbon nanomaterials, such as oxidized carbon nanotubes and graphene oxide. An adequate oxygen-surface chemistry development is necessary to obtain a good metallic load on the surface of the support. The supported organometallic complexes are stable an active catalysts in the reduction processes by means of hydrogen transfer.

The catalytic activity of those complexes bonded to the material, through the carboxylic and hydroxilic moieties, is similar or better than the corresponding homogeneous systems. In addition, the catalysts become stable in non-protected atmospheres, and the heterogenization allows the reuse of the catalysts due to the obtaining of the same times after the successive-cycles performance.

The local environment of the metal and the surface chemistry of the material determine the catalytic activity. Although all the NHC complexes-containing samples obtained complete conversions, only the faster catalysts where those which presented an adequate distribution of oxygen groups and structural defects. An excessive oxidation which generates free carboxylic acids, or ineffective which does not provide the required surface oxygen or defects on the material, leads to less efficient catalysts.

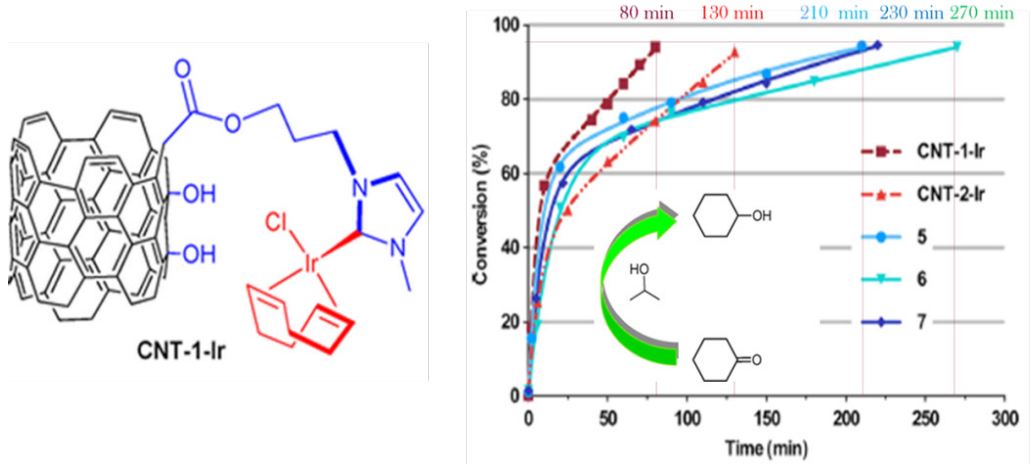

Figure 1. Structure of **CNT-1-Ir** sample and the catalytic activity in the reaction studied.

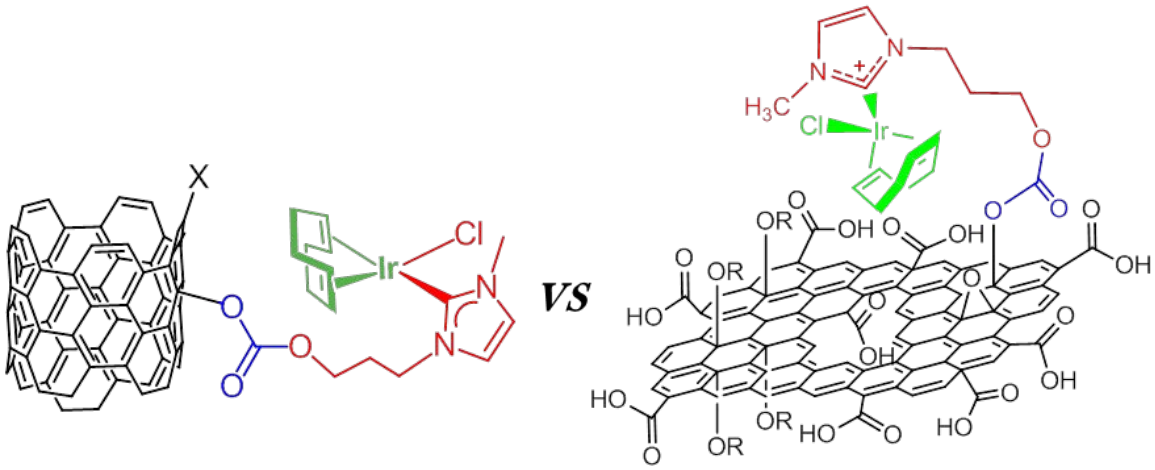

Figure 2. Structure of carbon hybrid materials functionalized in their OH groups

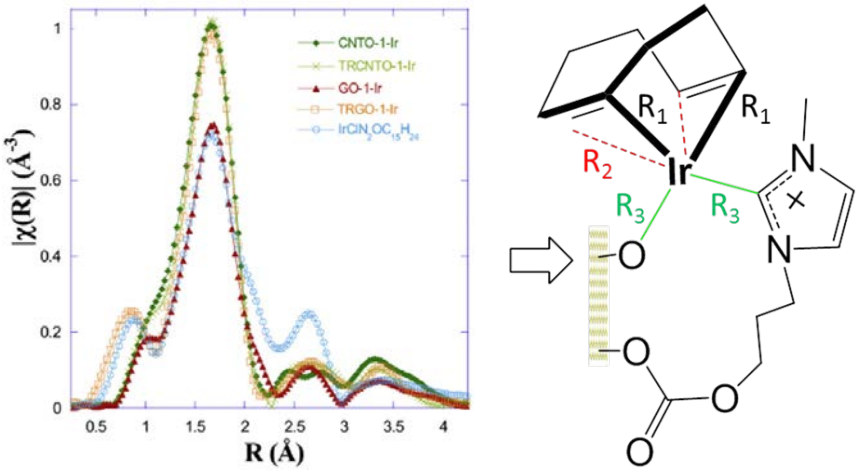

Figure 3. EXAFS data that allow revealing the actual structure of the hybrid systems covalently bonded to the carbon nanomaterials

RELATED PUBLICATIONS

[1] M. Blanco, P. Álvarez, C. Blanco, M.V. Jiménez, J. Fernández-Tornos, J.J. Pérez-Torrente, L.A. Oro, R. Menéndez. Enhanced Hydrogen-Transfer Catalytic Activity of Iridium N-Heterocyclic Carbenes by Covalent Attachment on Carbon Nanotubes. *ACS Catal*. **2013**, *3*, 1307-1317.

[2] M. Blanco, P. Álvarez, C. Blanco, N. Campos, D. Gómez, R. Ménendez. Influence of the alignment degree of CVD-grown carbon nanotubes on their functionalization and adsorption capacity. *Diamond and Related Materials*, **2013**, *37*, 1-7.

[3] M. Blanco, P. Álvarez, C. Blanco, M.V. Jiménez, J. Fernández-Tornos, J.J. Pérez-Torrente, L.A. Oro, R. Menéndez, Graphene–NHC–iridium hybrid catalysts built through –OH covalent linkage, *Carbon*, **2015,** 83, 21-31.

[4] M. Blanco, P. Álvarez, C. Blanco, M.V. Jiménez, J. Fernández-Tornos, J.J. Pérez-Torrente, L.A. Oro, J. Blasco, G. Subías. V. Cuartero, R. Menéndez. "Effect of structural differences of carbon nanotubes and graphene based iridium-NHC materials on the hydrogen transfer catalytic activity" *Carbon,* **2016**, 96, 66-74.

[5] J Blasco, V Cuartero, G Subías, M V Jiménez, J J Pérez-Torrente, L A Oro, M Blanco, P Álvarez, C Blanco, R Menéndez. "Local structure of Iridium organometallic catalysts covalently bonded to carbon nanotubes" *Journal of Physics, Conference series*. **2015**, Submitted.

[6] M. Blanco, P. Álvarez, C. Blanco, M.V. Jiménez, J. Fernández-Tornos, J.J. Pérez-Torrente, L.A. Oro, R. Menéndez. "Enhancing the hydrogen transfer catalytic activity of hybrid carbon nanotube-based NHC-iridium catalysts by increasing the oxidation degree of the nanosupport". *RSC Catalysis, Science and Technology*, **2015**, Submitted.

This thesis can be fully downloaded on www.uniovi.es

Thesis Review. Selective hydrogenation of α,β-unsaturated aldehydes and photodegradation of pollutants using catalysts based on carbon xerogels

E. Bailón-García

Presented in 2015, Department of Inorganic Chemistry, Faculty of Sciences, University of Granada, 18071 Granada, Spain.

Supervisors: F.J. Maldonado-Hódar and A.F. Pérez-Cadenas (University of Granada).

** Corresponding author: estherbg@ugr.es*

OBJECTIVES AND NOVELTY

The overall research objective of this study was the development of new synthesis methods of advanced materials based on carbon xerogels including structured pure carbon xerogels with controlled porosity and morfology as well as composites materials based on carbon xerogels-inorganic oxides and carbon xerogels-carbon nanofibers composites, in order to obtain suitable materials for very different applications: a) selective hydrogenation of α,β-unsaturated aldehydes, b) photocatalytic degradation of pollutants and c) biomedical applications. For the use of these materials in both catalytic applications, special attention is given to the optimization of parameters such as its microstructure, porosity, acidity, dispersion and metal-support interactions, type of active centers, etc. Thus, the synthesis methods previously developed in our laboratories have been adapted to optimize the properties of these materials to each of the proposed applications. These properties were also finally modified by different functionalization reactions to be used in medical applications. In this case, special attention to aspects like toxicity, biocompatibility, etc, were considered.

RESULTS

The selective hydrogenation of α,β-unsaturated aldehydes requires specific catalysts that favor the hydrogenation of the C = O group instead of the C = C one, more favorable kinetic and thermodynamically [1]. In the development of specific catalysts for such reaction, the influence of the support (inorganic supports, activated carbons, carbon xerogels and composites), the active phase (Pt, Ir or Ru) and the pre-treatment conditions (P_{H2}, T, agitation, contact time) have been studied. Intensive physical and chemical characterization of the supports and catalysts using a variety of complementary experimental techniques is performed. The reaction conditions and metal particle size is also optimized to ensure the absence of diffusional limitations and maximum performance. Thus it has been possible to establish correlations between the physicochemical properties of the supports and catalysts with its catalytic performance, more specifically, the yield to unsaturated alcohols (UA). The influence of the chemical and porous characteristics of both carbon and inorganic supports used to develop Pt-catalysts is studied. Using carbon supports (activated carbons and carbon xerogels), the performance of the derivatives Pt-catalysts strongly depends on the micro/mesoporous character of the supports and the presence of impurities, namely inorganics components. Mesoporosity and acid impurities leads to a decrease of UA yields, thus best results were obtained with microporous carbon xerogels (Figure 1) [2,3]. Similar conclusions were obtained when using inorganic supports, mesoporosity favors secondary reactions (consecutive hydrogenations, cyclization, etc) inside the pores, while mainly Brönsted acidity strongly favour cracking reactions [3]. In such a basis, Al_2O_3 always provides worse results than TiO_2 as Pt-supported catalysts for citral hydrogenation, in spite of their similar porous and pH_{pzc} values, while the microporous carbon xerogel structured in microspheres provides the highest selectivity to unsaturated alcohol, even higher than other bibliographic results for monometallic catalyts.

This behavior also depends deeply on the pretreatment conditions of the catalyst, which determine the chemical and crystalline transformation as well as the active phase dispersion. In spite that Pt-sintering in general is favored by H_2-pretreatment regarding the He-ones [3], which should lead to a stronger catalyst deactivation, in the case of Pt/TiO_2 catalysts the catalytic performance is improved after the H_2-pretreatment (Figure 2). This is because the H_2 treatment favors simultaneously the partial reduction of the TiO_2 surface, in such a way that the combination Pt site/oxygen vacancy has been identified as the real selective catalytic site to UA during citral hydrogenation [4].

Another important factor to take into acount is the active phase and the particle size because this type of hydrogenation reactions is structure sensitives.

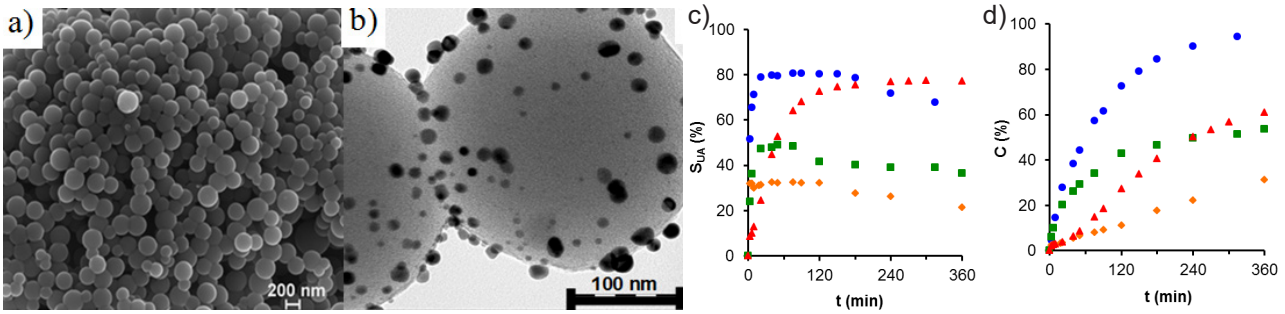

Figure 1. a) SEM images of carbon xerogel structured in microspheres and b) its corresponding Pt supported catalysts. c) Selectivity to unsaturated alcohols and d) conversion using Pt catalysts sopported on: TiO_2 (●), carbon xerogel A8 (▲), Al_2O_3 (■) and SiO_2 (◆).

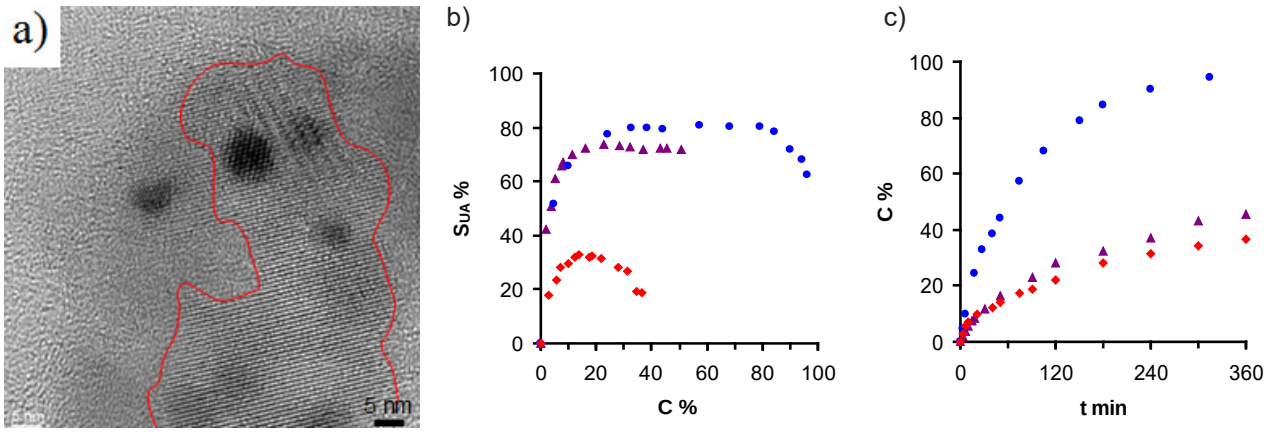

Figure 2. a) HRTEM images of Pt/TiO_2-H_2, b) selectivity to unsaturated alcohols and conversion after different treatment atmosphere of Pt/TiO_2: He (◆), H_2 (●) and He,H_2 (▲)

The metal particle size was optimized, for that; Pt-catalyst was pretreated under different experimental conditions obtaining Pt particles size from 2 to 10 nm. After test in the selective hydrogenation of citral it was pointed out that the optimum particle size is around 8 nm. Regarding the metal phase, a series of monometallic Pt, Ir and Ru-catalysts deposited on carbon xerogel microspheres was prepared, exhaustively characterized and used in the selective hydrogenation of citral. A similar metal particle size is obtained in all cases after He-pretreatment, allowing the comparison between metals; the catalytic activity increases in the sense Ir < Ru < Pt [5]. Sintering is favoured when catalysts are pretreated in H_2-flow leading to an important loss of activity, especially for Ru-catalysts. Pt and Ir-catalysts are more selective than Ru-catalysts, reaching selectivity values to unsaturated alcohols of around 80%. Thus, in terms of yields to these valuable products Pt-catalysts seem to be the most appropriate active phase. Nevertheless, reutilization experiments showed that Ir-catalyst maintained the catalytic performance while a severe deactivation is observed for Pt-catalysts. Deactivation was related with the chemisorption of CO or CO-evolving molecules on the Pt-surface.

These results open new opportunities in the preparation of highly selective hydrogenation catalysts combining the ability of TiO_2 to produces specific active site for citral adsorption through the C = O bond and the developed porosity and fitted surface chemistry (basicity) of carbon materials. The sol-gel synthesis procedure guarantees the purity of these supports avoiding interferences of the mineral matter present on classical ACs. The high surface areas of carbon xerogels facilitate the dispersion of the titanium dioxide particles and their reduction so, maximizing the strong metal-support interactions (SMSI effect) and Pt-dispersion.

So that, new carbon xerogels-inorganic oxide (ZrO_2, TiO_2, SiO_2, V_2O_5 and CeO_2) composites were prepared and used as Pt-support to develop catalysts for the selective hidrogenation of citral, obtaining specific and high active catalysts for the selective C=O hydrogenation of α,β-unsaturated aldehydes (more than 95 % of S_{UA} at total conversion). The synthesis method of these composites comprises resorcinol and formaldehyde polimerization in an organic medium simultaneously with the hydrolisis of a metal alkoxide precursor of the inorganic oxide. This method, was recently patented [6-8], and consists in an orderly and efficient sequence of specific steps that determine the final catalytic properties of these materials, for example the use of surfactant compounds, strict control of the polymerization temperature and stirring speed, a very slow addition of reactants or the use of microwave for the drying step. Under these conditions a very high dispersion of the metal oxide in the carbon xerogel matrix is achieved, maximizing the metal-support interactions in the resulting supported catalysts, which allows to obtain very high activities and selectivities at relatively mild reaction conditions, avoiding the use of supercritical solvents or bimetallic catalysts.

Given the nature of TiO_2/C composite materials, the study of their applications in photo-catalysis, specifically degradation processes of typical water pollutants such as azo dyes are further raised. The objective here was to optimize the material for enhanced its performance under visible radiation, but also carried out experiments using ultraviolet radiation. Alternatively, TiO_2 coating carbon xerogel spheres are also prepared (Figure 3). This TiO_2 coating is stable enough for use in the catalytic conditions tested. The crucial step is the pre-gelation of resorcinol-formaldehyde and the formation of nanostructures prior to coating. These new materials have been tested in the photo-degradation of Orange G using visible light obtained very good results. Results were compared in basis of decolourization, TOC analysis to determine the formation of oxidation intermediates and toxicity of the corresponding solutions using a standard method with luminescent bacteria (Vibrio Fisheri, NRRL-B-11177, in accordance with the European guideline ISO 11348-2:2007). The hydrophobic/hydrophilic nature of this material allows its precipitation in aqueous solution after completion of the decontamination process, which enables an easy separation of the photocatalyst after the reaction, with the advantage that this means in real applications.

Considering the progressive advance of the use of carbon materials in biomedical applications, and given that no references of the use of these materials in such applications have not been found despite the excellent properties of carbon aerogels and xerogels, a new line is also opted for studied during a stay at the University of Trieste, under the supervision of Prof. Maurizio Prato, one of the great specialists in these issues. For this, different carbon-based xerogel composites (gel materials and carbon gel-carbon

nanofibers, Figure 4a) were functionalized through reactions known as Tour and Prato (addition of aryldiazonium salts generated in situ and 1,3-dipolar cycloaddition of azomethine ylides, respectively) reaching high levels of functionalization compared with other materials commonly used in this field. Results of toxicity studies of such samples, evaluated in the presence of osteocytes, show the null toxicity of the samples . In addition, samples were not only non-toxic but also a cell growth was also observed increasing the concentration of carbon material in the culture medium, indicating a beneficial effect of the carbon material in the cell growth (Figure 4b). Therefore, this study points out that carbon xerogels could be interesting materials for biological applications, showing no toxicity due to their high purity and allowing high degrees of functionalization, which opens a new and very interesting field for the application of these carbonaceous materials.

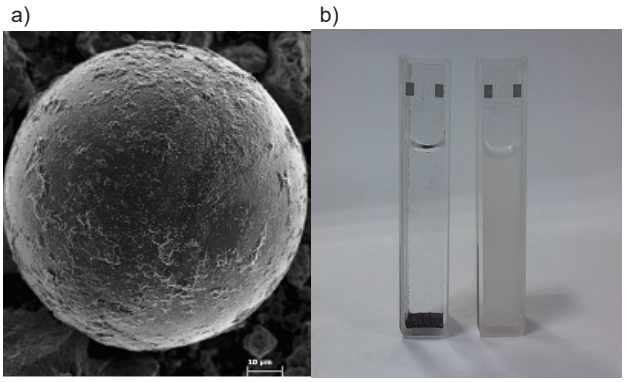

Figure 3.- a) SEM images of carbon xerogel microspheres coated with TiO_2 and b) suspensions of the photo-catalysts after reaction. Left (carbon xerogel microspheres coated with TiO_2); right (P25).

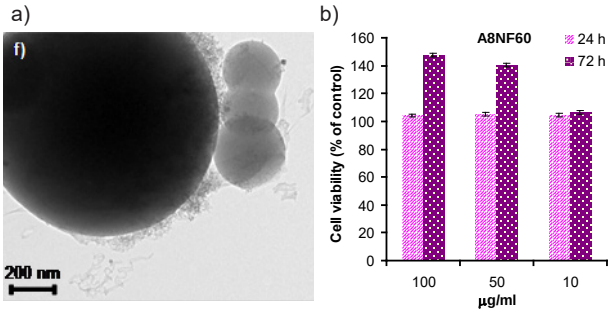

Figure 4.- a) TEM microphotograph of carbon gel-carbon nanofibers composite and b) LDH assay after incubation with carbon materials in fibroblast cell line at different carbon concentration for indicated times.

CONCLUSIONS

Different series of materials, including pure carbon xerogels and carbon – inorganic oxides composites were synthesized and deeply characterized. Their characteristics were fitted to a determined application. Catalysts to be used in the selective hydrogenation of citral and photocatalysts for the degradation of pollutant in water solutions were developed. Some samples were also applied for medical applications.

Hydrogenation catalysts were prepared by impregnation of the corresponding carbon-based supports with transition metals (Pt, Ir, Ru). Experimental parameters (T, PH_2, stirring, etc) were previously optimized and then, the physicochemical characteristics of catalysts were also fitted in order to obtain a high yield of unsaturated alcohols. The combination of carbon xerogels with TiO_2 provides a synergetic effect when used as Pt-support enhancing the S_{UA} up to 90%.

These materials also present very high photocatalytic activity for the degradation of pollutants in water. Again, a synergetic effect between both phases avoiding recombination of electrons, lowering the band-gap of the photocatalyst and favouring the adsorption of pollutants by increasing the porosity and surface area, permit a high performance and the use of visible radiation.

Finally, some of these materials were functionalized through reactions known as Tour and Prato. Results of toxicity studies, evaluated in the presence of osteocytes, show the null toxicity of the samples. Osteocites growth is favoured by increasing the carbon concentration. These samples can be used therefore also for the development of biological tissues.

RELATED PUBLICATIONS

[1] Bailón-García E, Maldonado-Hódar F.J., Pérez-Cadenas A.F., F. Carrasco-Marín, Catalysts supported on carbon materials for the selective hydrogenation of citral, Catalysts, 2013; 3, 853-877.

[2] Bailón-García E, Maldonado-Hódar F.J., Pérez-Cadenas A.F., F. Carrasco-Marín, Development of carbon xerogels as alternative Pt-supports for the selective hydrogenation of citral, Catal. Commun., 2014; 58, 64-69.

[3] Bailón-García E, Maldonado-Hódar F.J., Pérez-Cadenas A.F., F. Carrasco-Marín, Microspheres of carbon xerogel: An alternative Pt-support for the selective hydrogenation of citral, Appl. Catal. A: Gen., 2014; 482, 318-326.

[4] Bailón-García E, Maldonado-Hódar F.J., Pérez-Cadenas A.F., F. Carrasco-Marín, Influence of the pretreatment conditions on the development and performance of active sites of Pt/TiO_2 catalysts used for the selective citral hydrogenation, J. Catal, 2015; 327, 86-95.

[5] Bailón-García E, Maldonado-Hódar F.J., Pérez-Cadenas A.F., F. Carrasco-Marín, Selective hydrogenation of citral by noble metals supported on carbon xerogels: Catalytic performance and stability, Appl. Catal. A: Gen, 2015; In Press.

[6] Bailón-García E, Maldonado-Hódar F.J., Pérez-Cadenas A.F., F. Carrasco-Marín, Procedure to obtain carbon gel-metal oxide composites, catalyst and procedure to obtain unsaturated alcohols. Patent nº: ES2547777 A1

[7] Bailón-García E, Maldonado-Hódar F.J., Pérez-Cadenas A.F., F. Carrasco-Marín, Preparation process of photo-catalysts, obtainable photo-catalysts by this process and photodegradation procedure that uses them. Patent nº: ES2538627 A1.

[8] Bailón-García E, Maldonado-Hódar F.J., Pérez-Cadenas A.F., F. Carrasco-Marín, Photocatalyst compounds by zirconium oxide-carbon, preparation method and degradation of organic compounds. Patent nº: ES2540701 A1.

RESEÑA. Asociación Mexicana de Carbono A.C. - AMEXCarb

En la primera Reunión de Investigadores Latinoamericanos que se llevó a cabo dentro del Congreso Mundial Anual de Carbono (CMAC) en Río de Janeiro, Brasil, en julio de 2013, se propuso crear la Federación Latinoamericana de Carbono (FLC), la cual estaría conformada por las diferentes Asociaciones Latinoamericanas de Carbono. Además, se acordó que el primer Taller Latinoamericano de Materiales de Carbono para Medioambiente y Energía (TLMC) se llevaría a cabo en Punta del Este, Uruguay, en noviembre de 2014, el cual se llevó a cabo exitosamente. Debido a los compromisos establecidos en el CMAC, y después de determinar la pertinencia y factibilidad de fundar la **Asociación Mexicana de Carbono** (**AMEXCarb**), ésta fue oficialmente registrada el 12 de noviembre de 2014, justo antes de constituir la FLC con las asociaciones de Argentina, Brasil, Chile, Colombia, México y Uruguay dentro del TLMC.

Uno de los propósitos de la **AMEXCarb** es difundir los avances científicos relacionados con la formación, estructura, propiedades, comportamiento y aplicación tecnológica de los materiales a base de carbono. Lo anterior incluye, pero no está limitado a las siguientes líneas de investigación: Adsorción, Aplicaciones médicas y ambientales, Catálisis, Capacitores, Carbonizados, Compositos, Electroquímica, Grafito, Materiales magnéticos, Nanoestructuras de carbono, Síntesis de carbones activados, y Surfactantes.

Con el fin de cumplir con los objetivos de la AMEXCarb, se llevó a cabo el **Primer Congreso de la Asociación Mexicana de Carbono** (**AMEXCarb2015**) del 10 al 13 de noviembre del año en curso en las instalaciones del Instituto Potosino de Investigación Científica y Tecnológica A.C., en San Luis Potosí, S.L.P., al cual asistieron 99 personas. Se presentaron 3 conferencias plenarias, las cuales fueron impartidas por distinguidos investigadores: Profesores Robert Hurt (editor en jefe de la revista Carbon, Brown University, EUA), Diego Cazorla (Universidad de Alicante, España) y Gabriel Merino (CINVESTAV-Mérida, México), y 69 trabajos en extenso, dentro de los cuales 32 trabajos fueron presentados en forma oral y 37 en forma de poster. Además, se recibieron contribuciones de 29 instituciones de educación superior del país y de 4 empresas, las cuales representaron a 17 Estados de la Republica Mexicana y al Distrito Federal. Cabe mencionar que algunos de los trabajos presentados en el AMEXCarb2015 tuvieron la colaboración de instituciones extranjeras de los siguientes países: Brasil, Cuba, España, EUA, Francia, y Reino Unido.

La Asociación Mexicana de Carbono continuará trabajando con miras al AMEXCarb2017, así como para lograr su consolidación y reconocimiento a nivel nacional e internacional.

Dr. René Rangel Méndez

AMEXCarb
Presidente

Página Web:
www.ipicyt.edu.mx/AMEXCarb/index.html

Email:
amexcar@gmail.com

Fotografía del AMEXCarb2015

RESEÑA. Éxito de dos socios del GEC en la cuarta edición del Fondo de Emprendedores de la Fundación REPSOL

El pasado mes de septiembre se entregaron los premios de la 4ª convocatoria del Fondo de Emprendedores de la Fundación Repsol. Entre los galardonados se encuentra la Empresa de Base Tecnológica Xerolutions S.L., creada por Ana Arenillas y J. Ángel Menéndez, socios del GEC y antiguos editores de este Boletín.

El equipo editorial actual quiere aprovechar este espacio para dar la enhorabuena a Ana y Ángel y animar al resto de socios y lectores a participar en esta iniciativa de la Fundación Repsol, orientada a apoyar proyectos empresariales que aporten soluciones innovadoras en materia de energía, eficiencia y ahorro energético.

Ana Arenillas y J. Ángel Menéndez

Socios protectores del Grupo Español del carbón

Industrial Química del Nalón, S.A.
NalónChem

TECNOVAC
TECNOLOGÍA DE VACÍO S.L.

GRONTAL